Evaluating the triaxial strength of Misis fault breccia using artificial neural networks analysis

by S. Kahraman[1], M. Alber[2], O. Gunaydin[3], M. Fener[4]

Affiliation:
[1]Hacettepe University, Mining Engineering Department, Ankara, Türkiye
[2]Ruhr University-Bochum , Applied Geology Department, Bochum, Germany
[3]Adiyaman University, Civil Engineering Department, Adiyaman, Türkiye
[4]Ankara University, Geological Engineering Department, Ankara, Türkiye

Correspondence to:
S. Kahraman

Email:
sairkahraman@yahoo.com

Dates:
Received: 24 Mar. 2024
Revised: 19 May 2025
Accepted: 16 July 2025
Published: August 2025

How to cite:
Kahraman, S., Alber, M., Gunaydin, O., Fener, M. 2025. Evaluating the triaxial strength of Misis fault breccia using artifical neural networks analysis. *Journal of the Southern African Institute of Mining and Metallurgy*, vol. 125, no. 8, pp. 413–420

DOI ID:
https://doi.org/10.17159/2411-9717/3337/2025

ORCiD:
S. Kahraman
http://orcid.org/0000-0001-7903-143X
M. Alber
http://orcid.org/0000-0003-2488-7817
M. Fener
http://orcid.org/0000-0002-0464-5194
O. Gunaydin
http://orcid.org/0000-0001-7559-5684

Abstract

Falling into the weak rocks category, fault breccias have extremely poor engineering properties. These pebbles typically cause issues with slopes, subterranean construction, and building projects. Professionals will benefit from the creation of some predictive models for fault breccia triaxial strength, as smooth specimen preparation is typically challenging and time-consuming. The purpose of this study is to develop some predictive models for the differential stress (Δσ) based on physical and textural properties. Artificial neural networks were used to analyse data related to Misis fault breccia. Initially, models with moderate (noticeable, but not good) correlation coefficients were created using multiple regression analysis. After that, the regression models and three distinct artificial neuron network models were contrasted. Regression models are weaker and less trustworthy than artificial neuron network models, as demonstrated by this comparison. Pointed out is the practicality and ease of use of the artificial neuron network model with S-wave velocity and volumetric block proportion. Ultimately, it can be concluded that artificial neuron networks analysis provides a reliable indirect method for predicting the differential stress of Misis fault breccia.

Keywords

Misis fault breccia, triaxial strength, ultrasonic velocity, artificial neural networks

Introduction

Non-linear multivariable problems are typical in the geosciences. Regression analysis and conventional expert systems can occasionally fail to provide satisfactory solutions for such issues. Artificial neural networks (ANNs) are therefore frequently employed in the geosciences (Yuanyou et al., 1997; Yang, Zhang, 1998; Singh et al., 2001; Kahraman et al., 2005; Sonmez et al., 2006; Zorlu et al., 2008; Gunaydin et al., 2010, Dagdelenler et al., Marais, Aldrich, 2011, Sayadi et al., 2013; Khoshjavan et al., 2013; Basarir et al., Kahraman, 2016, etc.). Numerous geoscience studies have used ANNs, and the results have shown that ANN models perform well when solving multivariable problems.

Typically, fault breccias cause issues in applications involving rock engineering since they belong to a weak rock group. In order to solve the issues that arise when carrying out projects, it is crucial to understand or estimate the geomechanical properties of fault breccias. To prepare smooth specimens for standard tests, on the other hand, requires a lot of time, effort, and money, and fault breccias are typically not suitable for this. Deriving a few predictive models for the geomechanical characteristics of fault breccias will be beneficial because of this. Many researchers (Chester, Logan, 1986; Medley, 1994; Medley, Goodman 1994; Lindquist, Goodman, 1994; Ehrbar, Pfenniger, 1999; Goodman, Ahlgren, 2000; Buergi et al., 1999; Medley, 2001; Medley, 2002; Habimana et al., 2002; Laws et al., 2003; Sonmez et al., 2004; Sonmez et al., 2006; Coli, 2011; Afifipour, Moaref, 2014; Mahdevari, Maarefvand, 2017; Lu et al., 2019; Festa et al., 2019; Avsar, 2020; Caselle et al., 2024; Gayathridevi, Ray, 2025) have studied the characteristics of geologically complex rocks such as melanges and fault rocks. On the Ahauser fault breccia (Germany), Kahraman and Alber (2006; 2008) as well as Alber and Kahraman (2009) conducted the first study on the geomechanical properties of fault breccias. Later on, Kahraman et al. (2008) and Slatalla et al. (2010) assessed the geomechanical characteristics of the breccia from the Misis fault. Kahraman et al. (2010) examined how well the Cerchar abrasivity index worked in predicting the uniaxial compressive strength (UCS) and Young's modulus € of the Misis fault breccia.

Kahraman et al. (2008), investigated the triaxial strength of Misis fault breccia and developed an estimation equation for the differential stress (Δσ) using multiple regression analysis. However, the

correlation coefficient for this relationship was weak. In this work, artificial neural networks (ANNs) were utilised to analyse the triaxial strength of Misis fault breccia with the goal of creating more robust models. Fifty specimens were added to this study in addition to the eighteen from the previous investigation.

Sampling

For the experimental investigations, large blocks were taken from the Misis fault breccia (Ceyhan-Adana, Türkiye). The Misis fault's location map is displayed in Figure 1. Dolomitic limestone blocks embedded in a finely grained matrix of red claystone containing clay rich in iron make up the Misis fault breccia. From the large blocks in the lab, 68 test samples in total were cored. The test samples have a 61 mm diameter and a 2-2.5 length-to-diameter ratio (Figure 2).

Determination of textural properties

Each core sample's circumferential surface was scanned with the DMT CoreScan II to produce digital images. Using image analysis software, the volumetric block proportion (VBP), average block diameter (ABD), aspect ratio, and roundness of the blocks were calculated from the scanned images of the cores.

Estimation of volumetric block proportion

The volume of block partition (VBP) is calculated by dividing the volume of blocks or grains by the volume of rock mass. A few researchers have explained the VBP prediction methods and the uncertainties in predicting three-dimensional block size distributions from one- or two-dimensional measurements (Medley, Goodman, 1994; Goodman, Ahlgren, 2000; Medley, 1997; Medley, 2002; Haneberg, 2004). Blocks from the matrix are typically very difficult to separate, even though sieve analysis is the best technique. This is why it is common practice to estimate VBP using one- or two-dimensional methods like scanlines, geological mapping, and image analysis, or drill core/block intersection lengths. The circumferential surface scan images of the cores were processed and used to estimate VBP in this study. Figure 3 displays a sample's raw and processed images.

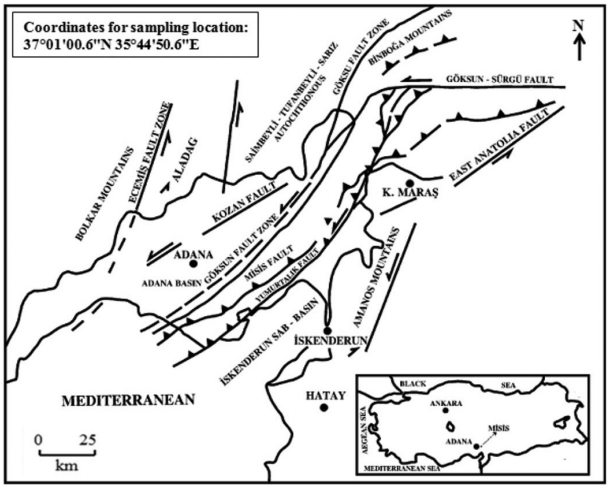

Figure 1—Location map of Misis Fault (Kahraman et al. 2015)

Figure 2—Some of the tested core samples

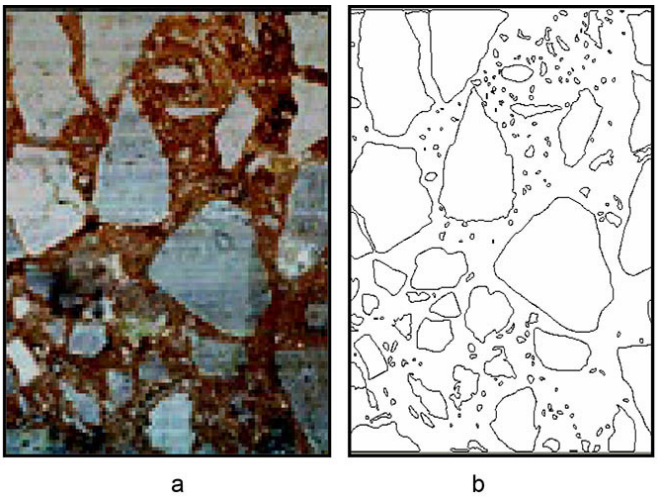

Figure 3—Original (a) and processed (b) images of a sample

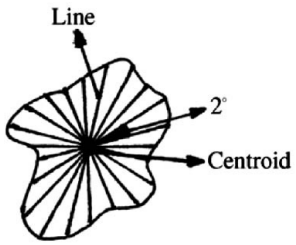

Figure 4—Illustration of the line passing through the 2° centroid of a block

Average block diameter

The length of the line that passes through each block's 2° centroid was used to estimate the two-dimensional diameter, which was assumed to be the same as the three-dimensional diameter (Figure 4). ABD values were then calculated by averaging these lines.

Aspect ratio of blocks

The length of the major and minor axes of an ellipse with an area equal to that of the block is called the aspect ratio, which characterises the elongation of blocks. Every block in the sample had its aspect ratio measured, and the average value was determined.

Roundness of blocks

Form factor is another way to define roundness. For a perfect circle, roundness equals 1. The roundness decreases as the shape moves away from circularity. Each block's roundness value in the sample was found, and the average value was computed. This is the roundness formula.

$$R = \frac{4\pi A}{p^2} \quad [1]$$

where R is roundness, A is the area of shape (mm^2), and p is the perimeter of shape (mm).

Table 1

Descriptive statistics of textural properties

Statistical parameter	Volumetric block proportion (%)	Average block diameter (mm)	Average aspect ratio of blocks	Roundness of blocks
Minimum	3.05	2.15	1.54	0.53
Maximum	80.93	10.22	2.22	0.85
Mean	33.14	5.00	1.93	0.66
Standard deviation	19.92	1.77	0.13	0.08
Variance	396.61	3.15	0.02	0.01
Skewness	0.05	0.68	-0.86	0.68
Number of samples	68	68	68	68

Table 2

Descriptive statistics of test results

Statistical parameter	Differential stress (MPa)	Density (g/cm^3)	P-wave velocity km/s)	S-wave velocity (km/s)
Minimum	26.40	2.35	3.71	1.69
Maximum	131.20	2.64	5.88	3.26
Mean	67.56	2.50	4.75	2.49
Standard deviation	23.05	0.06	0.45	0.34
Variance	531.12	0.01	0.20	0.12
Skewness	0.52	0.14	0.32	-0.43
Number of samples	68	68	68	68

Experimental studies

Prior to conducting triaxial compressive strength tests, each core sample underwent a density test and an ultrasonic test.

Density test

Density was calculated using samples of smooth core. Averaging multiple calliper readings allowed for the calculation of the specimen volume. A balance that could weigh the specimens precisely to within 0 points of the sample mass was used to determine their mass. The specimen mass to volume ratio was used to calculate the density values.

Ultrasonic test

To test the samples' elastic qualities, the USG 40 ultrasonic generator, made in Pirna, Germany, by Geotron GmbH, was employed. For the measurements, a 250 kHz ultrasonic transducer was employed. The ultrasonic tests yielded P- and S-wave velocities.

Triaxial compressive strength test

A stiff testing machine was used to perform the triaxial compression tests on smooth core specimens. The tests used confining pressures ranging from 1 MPa to 10 MPa. The triaxial cell of the Hoek-Franklin type has a capacity of about 70 MPa, while the load frame has a capacity of 4600 kN. Tests involved constant observation of the axial load and axial displacement. Two extensometers are used to measure axial deformation. Using an MTS Teststar IIm controller, the servo-hydraulics are controlled at high speed and in closed loop to operate the testing system. It is possible to use computed signals, such as stress or strain, or variable feedback signals, such as force or displacement, as control modes with this closed-loop control. However, this feature of the system has not been used in this study. The sample is loaded in axial strain control at a rate of 10^{-5} mm/mm/s beyond peak strength after being simultaneously loaded laterally and axially to the selected confining stress level.

Assessment of the results

Table 1 provides the textural characteristics of the tested samples along with statistical analyses. The values of VBP vary from 3.05 per cent to 80.93 per cent. The values of ABD vary from 2.15 per cent to 10.22 per cent. Blocks have aspect ratios ranging from 1.54 to 2.22. Blocks range in roundness from 0.53 to 0.85. Table 2 provides descriptive statistics of the physico-mechanical test results. The differential stress readings fall between 26.40 and 131.20 MPa. The density values are between 2.35 and 2.64 g/cm^3. The values of P-wave velocity span from 3:71 km/s to 5:88 km/s. The range of values for S-wave velocity is 1.69 km/s to 3.26 km/s.

The triaxial compressive test results were used to plot the Mohr stress circles. As illustrated in Figure 5, the stress circles are not uniform, and the failure envelope derived from these circles will not be trustworthy. Normally, as the confining stress increases (σ_3), the vertical stress (σ_1) increases steadily, and the Mohr circles shift to the right. Such unconformities frequently occur in geologically complex materials such as fault breccias. The inconsistent trend is expected, given the varying textural characteristics of the samples. In geologically complex materials such as breccias, the differential stress ($\Delta\sigma = \sigma_1-\sigma_3$) at failure can be a useful tool for determining the triple strength. This is why the failure envelope was not used in the analysis; instead, the $\Delta\sigma$ was used.

Regression analysis

The intercorrelations between the test results and the textural characteristics are displayed in a correlation matrix. There are no significant correlations between the independent parameters and the dependent parameter ($\Delta\sigma$), as Table 3 illustrates. This suggests that there is more than one parameter that influences the $\Delta\sigma$. According to a prior investigation (Kahraman et al., 2008), the strength range of block and matrix values is wide. This could be the cause of the absence of associations. The varying textures of the samples could be another factor. Therefore, in order to derive strong correlations, multivariable analysis is required.

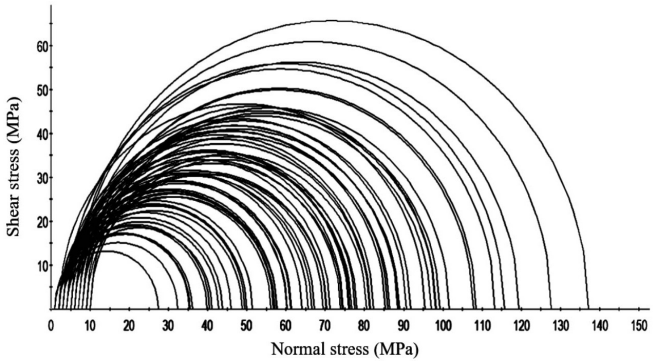

Figure 5—Mohr stress-circles

Alternative prediction models for the Δσ were examined using stepwise regression analysis. The software was used to create the following four models.

$$\Delta\sigma = -6.98 + 29.90V_s \qquad r = 0.45 \qquad [2]$$

$$\Delta\sigma = 9.81 + 28.69V_s - 0.42VBP \quad r = 0.57 \qquad [3]$$

$$\Delta\sigma = -450.99 + 22.24V_s - 0.89VBP + 197.05\rho \quad r = 0.64 \qquad [4]$$

$$\Delta\sigma = -702.92 + 23.03V_s - 1.19VBP + 292.67\rho + 4.19ABD \quad r = 0.69 \qquad [5]$$

where, Δσ is differential stress (MPa), V_s is *S*-wave velocity (km/s), *VBP* is volumetric block proportion (%), ρ is density (g/cm^3), and ABD is average block diameter (mm).

The first model (Equation 2) has a weak correlation coefficient. The other models (Equations 3-5) have moderate correlation coefficients.

Artificial neural network analysis

Artificial neural networks (ANNs) are extremely simplified models of the human brain's nervous system. The basic processing components of these models are interconnected assemblies of neurons arranged in layers. As can be seen in Figure 5, every neuron

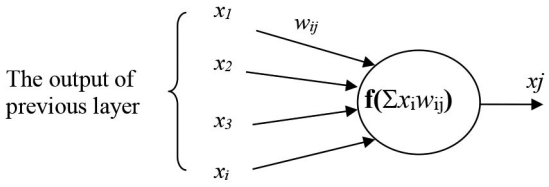

Figure 6—A simple block diagramme of a neuron

in one layer is connected to the neurons in the layer below it, and so forth. W_{ij} stands for 'weights,' and it describes the connection between the ith and jth layers. The potent tool for estimation and classification is provided by these connections between the layers. In order to minimise a predetermined cost function, these connections are optimised during the learning phase. The activation of a neuron is determined by its activation function, which is shown in Figure 6 as (f), and the weighted sum of its inputs is calculated to determine the neuron's output.

Multi layered perception (MLP) neural networks are the kind utilised in this investigation. In Figure 7, an MLP neural network is displayed. An input layer, one or more hidden layers, and an output layer make up MLP networks. There are many processing units (neurons) in each layer, and each unit is fully connected to units in the layer below it via weighted connections. The MLP uses nonlinear mapping functions to convert *i* inputs into *k* outputs.

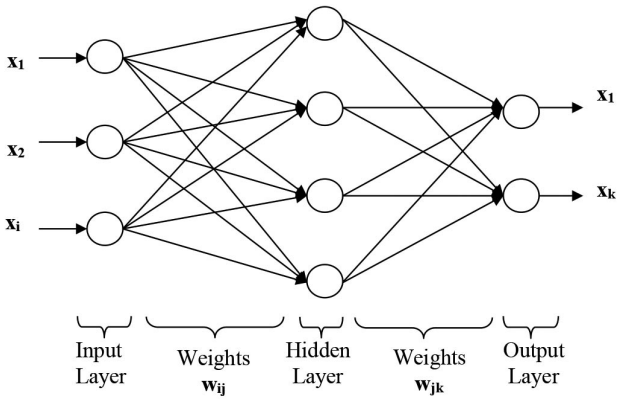

Figure 7—A multilayered perception neural network

Table 3

Correlation matrix for the data

	Differential stress (MPa)	Density (g/cm^3)	P-wave velocity km/s)	S-wave velocity (km/s)	Volumetric block proportion (%)	Average block diameter (mm)	Average aspect ratio of blocks	Roundness of blocks
Differential stress (MPa)	1.00							
Density (g/cm^3)	-0.08	1.00						
P-wave velocity km/s)	0.24	0.13	1.00					
S-wave velocity (km/s)	0.45	0.15	0.36	1.00				
Volumetric block proportion (%)	-0.38	0.81	0.24	-0.05	1.00			
Average block diameter (mm)	-0.03	-0.10	0.48	-0.19	0.20	1.00		
Average aspect ratio of blocks	-0.38	0.46	0.18	-0.12	0.60	0.11	00	
Roundness of blocks	0.26	-0.40	-0.38	0.03	-0.64	-0.43	-0.80	1.00

Table 4

The structures of the developed ANN models

Model no	Number of input neuron	Number of hidden neuron	Number of output neuron	Network type	Transfer function	Training parameters	Training algorithm
I	2	2	1	Feed-forward back propagation	Tanjant sigmoid	Learning rate: Adaptive gradient: 7.36 Epochs: 18	Levenberg-Marquardt backpropagation algorithm (trainlm)
II	3	5	1	Feed-forward back propagation	Tanjant sigmoid	Learning rate: Adaptive gradient: 227 Epochs: 18	Levenberg-Marquardt backpropagation algorithm (trainlm)
III	4	6	1	Feed-forward back propagation	Tanjant sigmoid	Learning rate: Adaptive gradient: 42.4 Epochs: 11	Levenberg-Marquardt backpropagation algorithm (trainlm)

Some investigators (Kumar, 2005; Altun et al., 2007) demonstrated that when data is highly skewed, ANN models do not always perform well in predictions. In order to minimise skewness in the data, a transformation such as power transformation can be applied prior to neural network analysis. The degree of symmetry of the normal distribution is gauged by its skewness. A symmetric distribution (one that is not skewed) is indicated by a skewness coefficient of 0. When a distribution is positively skew, it is skewed to the right; when it is negatively skew, it is skewed to the left. As demonstrated by Tables 1 and 2, the parameters' skewness values are typically low. Consequently, there is no need to transform or handle the data.

For the ANNs analysis, data from 68 rock samples were used. The network was trained, and several ANN models were developed using the data of the first group of 48. Ten of the data points were used for testing, and the other ten were used for validation.

Three regression models (Equations 3-5) mentioned in the aforementioned exhibit moderate correlation coefficient values. In order to evaluate these regression models against ANNs models, three distinct types of neural network structures were implemented in the MATLAB environment for the purpose of predicting the Δσ. The structures of the ANN models, i.e., the quantity of input layer neurons, hidden layer neurons, and output layer neurons are provided in Table 4. Table 4 also displays the training parameters and the algorithm used during the training phase.

A neural network with the structure 2-2-1 (Model I in Table 4) is used in the first trial. Using this structure, a model is built that illustrates the nonlinear relationship between the independent variables and the Δσ value. The model I is

$$\Delta\sigma = f(V_s, VBP) \quad [6]$$

A neural network is built in the second trial using the structure 3-5-1 (Model II in Table 4). The model II is

$$\Delta\sigma = f(V_s, VBP, \rho) \quad [7]$$

The third trial involves the construction of a neural network with the structure 4-6-1 (Model III in Table 4). The model III is

$$\Delta\sigma = f(V_s, VBP, \rho, ABD) \quad [8]$$

where, Δσ is differential stress (MPa), V_s is S-wave velocity (km/s), VBP is volumetric block proportion (%), ρ is density (g/cm^3), and ABD is average block diameter (mm).

Scatter plots indicating measured and predicted values can be used to display how well the derived models estimate values. When comparing estimated and observed data, a plotted data set should ideally have its points distributed around the 1:1 diagonal straight line. An accurate estimate is shown by a point that is on the line. Indicating non-linearity in one or more parameters, a systematic departure from this line can, for instance, show that larger errors typically go hand in hand with larger estimations. Plots of estimated Δσ versus observed Δσ are shown in Figures 8-10 for Models I, II, and III, respectively. The plots exhibit uniform point scattering around the diagonal line, indicating the plausibility of the models.

Comparison of regression and ANNs models

The correlation coefficients and standard error of estimates were used to compare the models produced by regression analysis and ANNs. Table 5 illustrates the moderate correlation coefficients of the regression models (Equations 3-5). Corresponding ANN models, however, have high correlation coefficients (Equations 6-8). Table 5 also provides the standard error of estimate values. ANN models

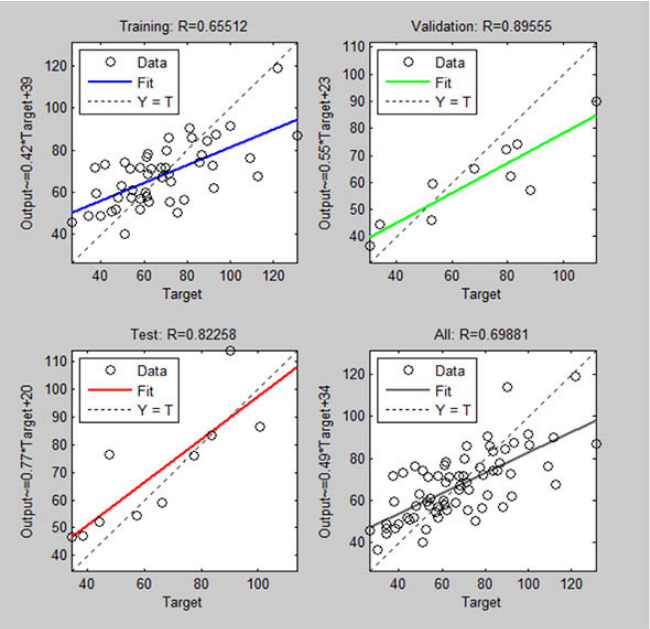

Figure 8—The plots of predicted versus measured Δσ for the Model I

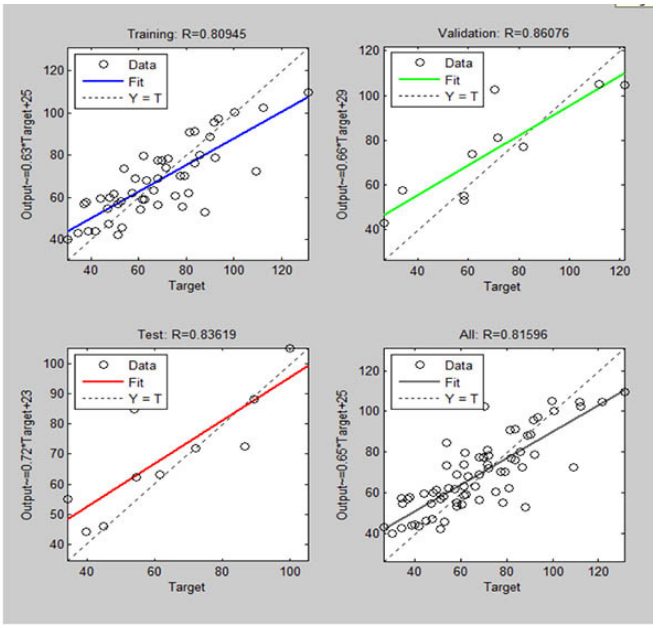

Figure 9—The plots of predicted versus measured Δσ for the Model II

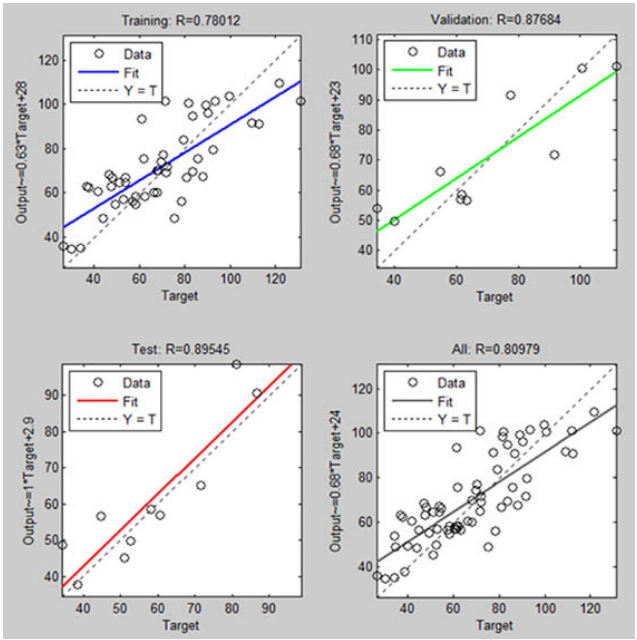

Figure 10—The plots of predicted versus measured Δσ for the Model III

exhibit lower standard error of estimates values in comparison to regression models. Comparison results reveal that ANNs models are strong and reliable for predicting the Δσ of fault breccia compared to the regression models.

Discussion

The correlations between Δσ and breccia characteristics such as S-wave velocity, VBP and average aspect ratio of blocks are examined, but these are weak, as shown in Table 3. The fact that the strengths of both the matrix and the blocks have wide ranges and the specimens have different textures is likely the cause of weak correlations. It is clear that the triaxial strength of the Misis fault breccia does not depend on one rock property. Multiple regression analyses were performed in anticipation of developing strong

Table 5

Correlation coefficients and standard error of estimates for the models produced from ANN and regression analysis

Model type	Model no	Coefficient of correlation (r)	Standard error of estimate
Regression models	Eq. (3)	0.57	19.18
	Eq. (4)	0.64	18.20
	Eq. (5)	0.69	17.10
ANNs models	Eq. (6)	0.82	13.93
	Eq. (7)	0.84	12.95
	Eq. (8)	0.89	8.68

models. However, the models derived from the multiple regression analysis show moderate correlation coefficients. An ANN analysis was then performed using the independent variables included in the regression models with moderate correlation coefficients. The developed ANN models were shown to be strong and reliable. The three ANNs models can be used to estimate the Δσ of the Misis fault breccia or similar breccias. Model I (Equation 6) is practical and easy to use because it has only two independent variables (S-wave velocity and VBP). Measuring S-wave speed is very simple. Determining VBP is quite difficult and time-consuming. Alternatively, VBP can be easily estimated from density as there is a good correlation between VBP and density, as shown in Table 3. The correlation equation is:

$$VBP = 277.6\rho - 660.8 \qquad r = 0.81 \qquad [9]$$

where, VBP is volumetric block proportion (%) and ρ is density (g/cm^3).

Conclusions

The predictability of the Δσ of the Misis fault breccia from physical and structural properties was examined using regression and ANN analysis. It was seen that there were no significant correlations between Δσ and independent variables. Some models with moderate correlation coefficients were derived through multiple regression analysis. Three different ANN models were constructed and compared with the regression models. Comparing the ANNs models with the regression models revealed that the ANNs models are stronger and more reliable than the regression models. The ANNs model (Equation 6) including S-wave velocity and VBP is practical and easy to use. A final note is that the Δσ of the Misis fault breccia can be reliably predicted from indirect methods using ANN analysis.

Acknowledgement

This study was supported by the Alexander von Humboldt Foundation.

References

Afifipour, M., Moarefvand, P. 2014. Mechanical behavior of bimrocks having high rock block proportion. *International Journal of Rock Mechanics and Mining Sciences,* vol. 65, pp. 40–48. https://doi.org/10.1016/j.ijrmms.2013.11.008

Alber, M., Kahraman, S. 2009. Predicting the uniaxial compressive strength and elastic modulus of a fault breccia from texture coefficient. *Rock Mechanics and Rock Engineering,* vol. 42, pp. 117–127. https://doi.org/10.1007/s00603-008-0167-x

Altun, H., Bilgil, A., Fidan, B.C. 2007. Treatment of skewed multi-dimensional training data to facilitate the task of engineering neural models. *Expert System with Applications*, vol. 33, pp. 978–983. https://doi.org/10.1016/j.eswa.2006.07.010

Avsar, E. 2020. Contribution of fractal dimension theory into the uniaxial compressive strength prediction of a volcanic welded bimrock. *Bull. Eng. Geol. Environ*. 2020, vol. 79, pp. 3605–3619. https://doi.org/10.1007/s10064-020-01778-y

Basarir, H., Tutluoglu, L., Karpuz, C. 2014. Penetration rate prediction for diamond bit drilling by adaptive neuro-fuzzy inference system and multiple regressions. *Engineering Geology,* vol. 173, pp. 1–9. https://doi.org/10.1016/j.enggeo.2014.02.006

Buergi, C., Parriaux, A., Franciosi, G., Rey, J.-Ph. 1999. Cataclastic rocks in underground structures – terminology and impact on the feasibility of projects (initial results). *Engineering Geology,* vol. 51, pp. 225–235. https://doi.org/10.1016/S0013-7952(97)00079-3

Caselle, C., Comina, C., Festa, A. Bonetto, S. 2024. Electrical resistivity tomography for the evaluation of Areal Block Proportion (ABP) in bimunits: Modelling and preliminary field validation. *Eng. Geol.* vol. 333, p. 107488. https://doi.org/10.1016/j.enggeo.2024.107488

Chester, F.M., Logan, J.M. 1986. Implications for mechanical properties of brittle faults from observations of the Punchbowl Fault Zone, California. *Pure and Applied Geophysics,* vol. 124, pp. 79–106. https://doi.org/10.1007/BF00875720

Coli, N., Berry, P., Boldini, D. 2011. In situ non-conventional shear tests for the mechanical characterisation of a bimrock. *International Journal of Rock Mechanics and Mining Sciences,* vol. 48, pp. 95–102. https://doi.org/10.1016/j.ijrmms.2010.09.012

Dagdelenler, G., Sezer, E.A., Gokceoglu, C. 2011. Some non-linear models to predict the weathering degrees of a granitic rock from physical and mechanical parameters. *Expert Systems with Application,* vol. 38, pp. 7476–7485. https://doi.org/10.1016/j.eswa.2010.12.076

Ehrbar, H., Pfenniger, I. 1999. Umsetzung der Geologie in technische Massnahmen im Tavetscher Zwischenmassive Nord. In Vorerkundung und Prognose der Basistunnels am Gotthard und am Lötschberg. Rotterdam, *Balkema*, pp. 381-394.

Festa, A., Pini, G.A., Ogata, K., Dilek, Y. 2019. Diagnostic features and field-criteria in recognition of tectonic, sedimentary and diapiric mélanges in orogenic belts and exhumed subduction-accretion complexes. *Gondwana Res*. 2019, vol. 74, pp. 11–34. https://doi.org/10.1016/j.gr.2019.01.003

Gayathridevi, K., Ray, A. 2025. Mechanical Characterization of Soil–Rock Mixture Under Varying Block Parameters, Matrix Properties and Matrix Water Content Using Destructive and Non-Destructive Testing. *Indian Geotech J* (June 2025) vol. 55, no. 3, pp. 1779–1794. https://doi.org/10.1007/s40098-024-01054-w

Goodman, R.E., Ahlgren, C.S. 2000. Evaluating safety of concrete gravity dam on weak rock: Scott Dam. *Journal of Geotechnical and Geoenvironmental Engineering,* vol. 126, no. 5, pp. 429–442. https://doi.org/10.1061/(ASCE)1090-0241(2000)126:5(429)

Gunaydin, O., Gokoglu, A., Fener, M. 2010. Prediction of artificial soil's unconfined compression strength test using statistical analyses and artificial neural networks. *Advances in Engineering Software,* vol. 41, pp. 1115–1123. https://doi.org/10.3390/app11041949

Habimana, J., Labiouse, V., Descoeudres, F. 2002. Geomechanical characterisation of cataclastic rocks: experience from the Cleuson–Dixence project. *International Journal of Rock Mechanics and Mining Sciences,* vol. 39, no. 6, pp. 677-93. https://doi.org/10.1016/S1365-1609(02)00042-4

Haneberg, W.C. 2004. Simulation of 3-D block populations to characterize outcrop sampling bias in block-in-matrix rocks (bimrocks). *Felsbau-Rock and Soil Engineering,* vol. 22, pp. 19–26.

Kahraman, S., Altun, H., Tezekici, B.S., Fener, M. 2005. Sawability prediction of carbonate rocks from shear strength parameters using artificial neural networks. *International Journal of Rock Mechanics and Mining Science,* vol. 43, no. 1, pp. 157–164. https://doi.org/10.1016/j.ijrmms.2005.04.007

Kahraman, S., Alber, M. 2006. Estimating the unconfined compressive strength and elastic modulus of a fault breccia mixture of weak rocks and strong matrix, *International Journal of Rock Mechanics and Mining Sciences,* vol. 43, pp. 1277-1287. https://doi.org/10.1016/j.ijrmms.2006.03.017

Kahraman, S., Alber, M. 2008. Triaxial strength of a fault breccia of weak rocks in a strong matrix. *Bulletin of Engineering Geology and the Environment,* vol. 67, pp. 435–441. https://doi.org/10.1007/s10064-008-0152-3

Kahraman, S., Alber, M., Fener, M., Gunaydin, O. 2008. Evaluating the geomechanical properties of Misis Fault Breccia (Turkey). *International Journal of Rock Mechanics and Mining Sciences*, vol. 45, pp. 1469–1479. https://doi.org/10.1016/j.ijrmms.2008.02.010

Kahraman, S., Alber, M., Fener, M., Gunaydin, O. 2010. The usability of Cerchar abrasivity index for the prediction of UCS and E of Misis Fault Breccia: Regression and artificial neural networks analysis. *Expert Systems with Applications*, vol. 37, pp. 8750–8756. https://doi.org/10.1016/j.eswa.2010.06.039

Kahraman, S., Alber, M., Fener, M., Gunaydin, O. 2015. An assessment on the indirect determination of the volumetric block proportion of Misis fault breccia (Adana, Turkey). *Bull Eng Geol Environ*, vol. 74, pp. 899–907. https://doi.org/10.1007/s10064-014-0666-9

Kahraman, S. 2016. The prediction of penetration rate for percussive drills from indirect tests using artificial neural networks. *J. South. Afr. Inst. Min. Metall*. vol. 116, pp. 793–800. https://www.saimm.co.za/Journal/v116n08p793.pdf

Khoshjavan, S., Khoshjavan, R., Rezai, B. 2013. Evaluation of the effect of coal chemical properties on the Hardgrove Grindability Index (HGI) of coal using artificial neural networks. *J. South. Afr. Inst. Min. Metall*. vol. 113, pp. 505–510. https://www.saimm.co.za/Journal/v113n06p505.pdf

Kumar, U.A. 2005. Comparison of neural networks and regression analysis: A new insight. *Expert System with Applications,* vol. 29, pp. 424-430. https://doi.org/10.1016/j.eswa.2005.04.034

Laws, S., Eberhardt, E., Loew, S., Descoeudres, F. 2003. Geomechanical properties of shear zones in the Eastern Aar Massif, Switzerland and their implication on tunnelling. *Rock Mechanics and Rock Engineering,* vol. 36 , no. 4, pp. 271–303. https://doi.org/10.1007/s00603-003-0050-8

Lindquist, E.S., Goodman, R.E. 1994. Strength and deformation properties of a physical model melange. In: Nelson PP, Laubach SE, editors. In *Proceedings of the 1st North American Rock Mechanics Symposium*. Rotterdam: Balkema, pp. 843–50. https://onepetro.org/ARMANARMS/proceedings-abstract/NARMS94/All-ARMS94/ARMA- 1994-0843/121172

Lu, Y.C., Tien, Y.M., Juang, C.H., Lin, J.S. 2019. Uncertainty of volume fraction in bimrock using the scan-line method and its application in the estimation of deformability parameters. *Bull. Eng. Geol. Environ*. 2019, vol. 79, pp. 1651–1668. https://doi.org/10.1007/s10064-019-01635-7

Mahdevari, S., Maarefvand, P. 2017. Applying ultrasonic waves to evaluate the volumetric block proportion of bimrocks. Arab. *J. Geosci.* 2017, vol. 10, pp. 204. https://doi.org/10.1007/s12517-017-2999-8

Marais, C., Aldrich, C. 2011. The estimation of platinum flotation grade from froth image features by using artificial neural networks. *J. South. Afr. Inst. Min. Metall.* vol. 111, pp. 81-85. https://www.saimm.co.za/Journal/v111n02p081.pdf

Medley, E.W., Goodman, R.E. 1994. Estimating the block volumetric proportions of melanges and similar block-in-matrix rocks (bimrocks). In Proceedings of the 1st North American Rock Mechanics Symposium. Rotterdam: *Balkema*, pp. 851–8. https://onepetro.org/ARMANARMS/proceedings-abstract/NARMS94/All-ARMS94/ARMA- 1994-0851/121194

Medley, E.W. 1994. The engineering characterization of melanges and similar block-in-matrix rocks (bimrocks). Ph.D. Dissertation. University of California at Berkeley, California. Ann Arbor, MI: UMI, Inc.

Medley, E.W. 1997. Uncertainty in estimates of block volumetric proportions in melange bimrock. In Proceedings of the International Symposium on Engineering Geology and The Environment. Rotterdam: *Balkema*, pp. 267–72.

Medley, E.W. 2001. Orderly characterization of chaotic Franciscan Melanges. *Felsbau-Rock and Soil Engineering,* vol. 19, pp. 20–33.

Medley, E.W. 2002. Estimating block size distribution of melanges and similar block-in-matrix rocks (bimrocks). In *Proceedings of the 5th North American Rock Mechanics Symposium*. Toronto, Canada: University of Toronto Press, pp. 509–16. https://www.geoengineer.org/bimrocks/files/Medley2002.PDF

Sayadi, A., Monjezi, M., Talebi, N., Khandelwal, M. 2013. A comparative study on the application of various artificial neural networks to simultaneous prediction of rock fragmentation and backbreak. *Journal of Rock Mechanics and Geotechnical Engineering*, vol. 5, pp. 318–324. https://doi.org/10.1016/j.jrmge.2013.05.007

Singh, V.K., Singh, D., Singh, T.N. 2001. Prediction of strength properties of some schistose rocks from petrographic properties using artificial neural networks. I*nternational Journal of Rock Mechanics and Mining Sciences,* vol. 38, pp. 269–84. https://doi.org/10.1016/S1365-1609(00)00078-2

Slatalla, N., Alber, M., Kahraman, S. 2010. Analyses of acoustic emission response of a fault breccia in uniaxial deformation. *Bulletin of Engineering Geology and the Environment,* vol. 69, pp. 455–463. https://doi.org/10.1007/s10064-010-0296-9

Sonmez, H., Gokceoglu, C., Tuncay, E., Medley, E. 2004. Relationship between volumetric block proportion and overall UCS of a volcanic bimrock. *Felsbau-Rock and Soil Engineering,* vol. 22, pp. 27–34.

Sonmez, H., Gokceoglu, C., Medley, E.W., Tuncay, E., Nefeslioglu, H.A. 2006. Estimating the uniaxial compressive strength of a volcanic bimrock. *International Journal of Rock Mechanics and Mining Sciences,* vol. 43, pp. 554-61. https://doi.org/10.1016/j.ijrmms.2005.09.014

Yang, Y., Zhang, Q. 1998. The applications of neural networks to rock engineering Systems (RES). *International Journal of Rock Mechanics and Mining Sciences,* vol. 35, no. 6, pp. 727–745. https://doi.org/10.1016/S0148-9062(97)00339-2

Yuanyou, X., Yanming, X., Ruigeng, Z. 1997. An engineering geology evaluation method based on an artificial neural network and its application. *Engineering Geology,* vol. 47, pp. 149–56. https://doi.org/10.1016/S0013-7952(97)00015-X

Zorlu, K., Gokceoglu, C., Ocakoglu, F., Nefeslioglu, H.A., Acikalin, S. 2008. Prediction of uniaxial compressive strength of sandstones using petrography-based models. *Engineering Geology,* vol. 96, pp. 141-158. https://doi.org/10.1016/j.enggeo.2007.10.009 ◆